2020 American Control Conference
Denver, CO, USA, July 1-3, 2020

Learning physical laws: the case of micron size particles in dielectric fluid

Ion Matei, Maksym Zhenirovskyy, Johan de Kleer, Christoforos Somarakis and John S. Baras

Abstract— **We address the problem of learning laws governing the behavior of physical systems. As a use case we choose the discovery of the dynamics of micron-scale chiplets in dielectric fluid whose motion is controlled by a set of electric potential. We use the port-Hamiltonian formalism as a high level model structure that is continuously refined based on our understanding of the physical process. In addition, we use machine learning inspired models as low level representations. Representation structure is key in learning generalizable models, as shown by the learning results.**

I. Introduction

Accurate and reliable modeling of complex physical processes is often an unfeasible task. The modeling challenges can stem from either an incomplete understanding of the physical process, the high complexity of the process, or lack of access to all system parameters. When accurate models are needed, machine learning (ML) inspired algorithms are an avenue to augment our partial models. In this paper we use a variety of ML models to (re-)discover the physical laws governing the behavior of chiplets in dielectric fluid. The chiplets' motion is a function of their potential energy which, in turn, is depends on the electric potentials applied through a set of electrodes. Having an accurate model for this type of physical process enable the design of feedback control that can lead to high throughput in applications of nanotechnology, expanding the printing technology for advanced functional output inks [4], [5], [9], [10]. Yet, training generalizable ML models requires large data sets and/or non-trivial regularization functions that constrain the parameter search space. Typical machine learning regularization functions based on L_1 or L_2 norms do not necessarily guide the search towards the correct parameters, since all they do is limit the magnitude of the model parameters or induce sparse models. A more appropriate alternative is to use our knowledge about the physical process to come up with a regularization function that impose some structural properties. We show in the paper a variety of ML inspired models that increasingly add more structure and we discuss their impact on the learning results, their usability and generalizability.

We use the port-Hamiltonian formalism to impose structure on models. This is a well-known general framework for representation and analysis of complex dynamical systems [13], [14], [15]. Port-Hamiltonian systems are based on a known energy function (Hamiltonian) and the interconnection of atomic structure elements (e.g., inertia, springs and dampers for mechanical systems) that interact by exchanging energy. They provide an energy-consistent description of a physical system, having the property that a power conservative interconnection of port-Hamiltonian systems is again a port-Hamiltonian system [2]. In addition to modeling, the port-Hamiltonian formalism is particularly suited for finding symmetries and conserved quantities [11]. It allows one to find conserved quantities, in addition to the Hamiltonian, called Casimir functions [13], by examining conditions related to the port-Hamiltonian system at hand, which can lead to model simplification (reduction). Moreover, finding parameterized symmetries, i.e., Lie groups of transformations, can lead to data generation without experimentation, as well as provide insight on the modeling equations of the system itself [1], [12]. We use the port-Hamiltonian representation as a high level model that will be successfully refined by imposing additional structure; structure that will indirectly induce regularization functions for the learning process.

Paper structure: In Section II we describe the physical process of interest and the experimental setup used to generate data and validate models. Section III introduces the port-Hamiltonian representation of the chiplet dynamics, a discrete symmetry map that characterizes the chiplet dynamics and the description of the high-detail simulation setup that was used to learn physical quantities needed by the model. In Section IV we discuss the set of representations for the chiplet dynamics and the learning results. We show how for this problem we can re-discover the discrete symmetry directly from data, and how the representations can be extended to the 2D case.

II. Problem description

Our goal is to learn/understand how an electric field manipulated by changing the potentials of a set of electrodes affects the motion of particles of dimensions $300\mu m \times 200\mu m \times 50\mu m$. The particles are submerged in a dielectric fluid which is a dielectric carrier (Isopar-M). Such a fluid has low conductivity and allows for long-range Coulomb interactions. In this fluid, chemically charged chiplets can be manipulated with both electrophoretic and dielectrophoretic forces. The electric field is manipulated by varying the potential of a set of electrodes. Spiral electrodes patterns were created using four non-crossing metal line (electrodes) which induce radial electrodes periodicity. For each of the four spirals, the four non-crossing metal lines are controlled by +/- 400 V amplifiers driven by a computer. The electrostatic potentials

This material is based, in part, upon work supported by the Defense Advanced Research Projects Agency (DARPA) under Agreement No. HR00111990027.

Ion Matei, Maksym Zhenirovskyy, Johan de Kleer and Christoforos Somarakis are with the Palo Alto Research Center, Inc. (PARC) (emails: imatei@parc.com, mzhenirovskyy.parc@gmail.com, dekleer@parc.com, csomarak@parc.com). John S. Baras is with the University of Maryland, College Park, MD (email: baras@umd.edu).

Authorized licensed use limited to: Palo Alto Research Center (PARC). Downloaded on August 26,2020 at 01:39:16 UTC from IEEE Xplore. Restrictions apply.

created in these electrodes, while limited in spatial patterns, are rich in temporal patterns. The spiral arrangement of the electrodes induces a radial motion of the chiplets (away or towards the center of the spiral). A detailed description of the experimental setup can be found in [9].

In [9], [10] we showed how we can design potential patterns for the chiplets motion control. We initially used an optimization based open loop control that generated a sequence of electrode potentials for moving the chiplets. We showed that the control pattern is periodic, and it can be reproduced using one basis function over one period, through translations and sign inversions. Denoting by $v_1(x)$ denote electrode 1's voltage, we obtained that v_1 is spatially periodic, with a period of $X = 800\mu m$, that is $v_1(x) = v_1(x + nX)$, for $n \in \mathbb{Z}$. Moreover, the voltage pattern over one period is given by the base function $\Psi : [0, X] \rightarrow [-400, 400]$. Hence, v_1 is generated according to the rules

$$v_1(x) = v_1(x + nX),\ v_1(x) = \Psi(x),\ n \in \mathbb{Z},\ x \in [0, X) \quad (1)$$

By analyzing the correlation between v_1 and the rest of the electrodes voltages, we see that the last three electrodes voltages can be expressed as

$$v_2(x) = -v_1(x + \delta), v_3(x) = v_1(x + 2\delta), v_4(x) = -v_1(x - \delta) \quad (2)$$

where $\delta = 200\mu m$. Therefore, for moving the chiplet in a positive direction a position dependent control input can be generated using only the base function $\Psi(x)$ and the rules (1)-(2). The control patterns above correspond to a positive motion direction (left to right). Similar rules in terms of $\Psi(x)$ can be determined to move the chiplet in the opposite direction.

III. Dynamical model

We consider the single chiplet scenario and model the physics of the interaction between the chiplet and the electric field using a particle based, port-Hamiltonian formalism [8]. We consider a set of $N + 1$ particles indexed from 0 to N, where the 1 through N particles represent the electrodes, and the 0 particle represents the chiplet. The particle dynamics can be represented in port-Hamiltonian formalism as

$$\dot{\boldsymbol{p}} = R(\boldsymbol{q})\frac{\partial \boldsymbol{H}(\boldsymbol{p},\boldsymbol{q})}{\partial \boldsymbol{p}} + J\frac{\partial \boldsymbol{H}(\boldsymbol{p},\boldsymbol{q})}{\partial \boldsymbol{q}} \quad (3)$$

$$\dot{\boldsymbol{q}} = -J^T\frac{\partial \boldsymbol{H}(\boldsymbol{p},\boldsymbol{q})}{\partial \boldsymbol{p}}, \quad (4)$$

where $\boldsymbol{p}$ is the vector of particle momenta, $\boldsymbol{q}$ is the vector of relative positions between the particle and the electrodes, $R(\boldsymbol{q})$ is a dissipative matrix, J is a matrix reflecting the particle interaction topology, and H is the Hamiltonian (energy) function. In particular, we have $\boldsymbol{p} = [p, p_1, \ldots, p_N]^T$ and $\boldsymbol{q} = [x_1 - x, \ldots, x_N - x]^T$, where x is the chiplet position (measured at the center of mass), and x_i are the electrode positions. The total energy can be expressed as $\boldsymbol{H}(\boldsymbol{p},\boldsymbol{q}) = \boldsymbol{K}(\boldsymbol{p}) + \boldsymbol{U}(\boldsymbol{q})$, where $\boldsymbol{K}(\boldsymbol{p})$ is the potential energy of the particles $\boldsymbol{K}(\boldsymbol{p}) = \sum_{i=0}^{N} K_i(\boldsymbol{p})$, where index 0 corresponds to the chiplet, $K_i(\boldsymbol{p}) = \frac{p_i^2}{2m_i}$ with m_i being the particle i mass, and $\boldsymbol{U}(\boldsymbol{q};\boldsymbol{v})$ is the potential energy given by $\boldsymbol{U}(\boldsymbol{q};\boldsymbol{v}) = \sum_{j=1}^{N} U_j(\boldsymbol{q};\boldsymbol{v})$, where $U_j(\boldsymbol{q};\boldsymbol{v})$ is the potential energy between the chiplet and electrode j, and $\boldsymbol{v} = [v_1, \ldots, v_N]^T$ is the vector of all electrode potentials. We assume that the chiplet is roughly at a constant height (at the surface of the PFA film), hence we neglect any vertical forces that may affect the chiplet motion. This assumption proved to be valid in experiments [9]. To represent the potential energy, we use a capacitive-based electrical circuit that lumps the interaction between the electrodes and the chiplet. Such a circuit is shown in Figure 1, where four electrodes are depicted. The chiplet and the electrodes act as metal plates; hence the capacitances of these capacitors are dependent on the chiplet position. As expected, the maximum values are attained when the chiplet's position maximizes the overlap with the electrodes. A small "leakage" capacitor C_ε is included to account for all the stray capacitance to the environment. Therefore, the

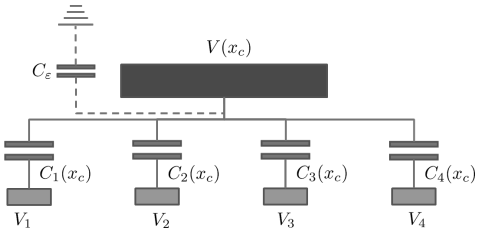

Fig. 1. Capacitive-based electrical circuit describing the interaction between the chiplet and four electrodes. The green rectangles depict the electrodes, while the purple rectangle represents the chiplet. The capacitances vary with the chip position whose center is denoted by (x_c, y_c). A small capacitance C_ε describes the interaction of the chiplet with the ground.

potential energy between the chiplet and each electrode can be expressed as $U_j(\boldsymbol{q}) = \frac{1}{2}C(q_j)(v_j - V(x))^2$, where $C(q_j)$ is the capacitance between the chiplet and electrode j that depends on the distance between the chiplet and electrode, v_j is the electric potential at electrode v_j, and $V(x)$ is the potential at the chiplet. The capacitance function $C(q)$ is a symmetric, positive function that converges to zero as the magnitute of q increases. The steady state chiplet potential is given by $V(x;\boldsymbol{v}) = \left(1/\left(\sum_{j=1}^{N} C(q_j) + C_\varepsilon\right)\right)\left(\sum_{j=1}^{N} C(q_j)v_j\right)$, where C_ε is a small leakage capacitance.

Since the electrodes are at fixed locations $\{x_i\}_{i=1}^{N}$, their kinetic energy is zero, hence we obtain the simplified port-Hamiltonian representation

$$\dot{p} = \mu\frac{\partial K_0(p)}{\partial p} + J\frac{\partial \boldsymbol{U}(\boldsymbol{q})}{\partial \boldsymbol{q}}, \quad (5)$$

$$\dot{\boldsymbol{q}} = -J^T\frac{\partial K_0(p)}{\partial p}, \quad (6)$$

where μ denotes the viscous friction coefficient determined from the chemical properties of the isopar-M solution and the geometry of the chiplet. In addition, the topology dependent matrix J is the vector of all ones, namely $J = [1, 1 \ldots, 1]^T$. The port-Hamiltonian representation can be brought to a more familiar form by representing the chiplet dynamics in terms of the chiplet's position. In particular, we have

$$m\ddot{x} = \mu\dot{x} + \frac{\partial \boldsymbol{U}(x;\boldsymbol{v})}{\partial x}, \quad (7)$$

Authorized licensed use limited to: Palo Alto Research Center (PARC). Downloaded on August 26,2020 at 01:39:16 UTC from IEEE Xplore. Restrictions apply.

where $\boldsymbol{U}(x;\boldsymbol{v}) = \frac{1}{2}\sum_{j=1}^{N} C(x_j - x)(v_j - V(x;\boldsymbol{v}))^2$ is the chiplet potential energy. Due to very small chiplet mass m, the acceleration effect is negligible as compared to the effects of the viscous friction and the potential energy.

In addition to the dynamical model, we are interested in other properties such as symmetries and conserved quantities. We recall that a symmetry is a diffeomorphism that maps a solution of a dynamical system to another solution [6]. These properties give additional insight into a system behavior and provide the avenue for generating data without the need of experimentation. The following results introduces a discrete symmetry map for the dynamics (7).

Proposition 3.1: Let the map $\Gamma : \mathbb{R}^{N+1} \to \mathbb{R}^{N+1}$ be defined as $\Gamma(x,\boldsymbol{v}) = (-x, P\boldsymbol{v})$, where $\boldsymbol{v}$ is the vector of all electrodes potentials and P is a rotational matrix that produces a 180 degree rotation. Without loss of generality, consider an even number of electrodes whose positions are symmetrically distributed around zero. Then Γ is a symmetry map for the dynamics (7).

Proof: For convenience, let the electrodes positions be denoted by $\{x_{-M},\ldots,x_{-1},x_0,x_1,\ldots,x_M\}$ with corresponding electric potentials $\{V_j\}_{j=-M}^{M}$, for some positive integer $N = 2M+1$. The proof is based on showing that $\boldsymbol{U}(x;\boldsymbol{v}) = \boldsymbol{U}(-x;P\boldsymbol{v})$ and applying the chain rule. We first note that due to the symmetry of $C(q)$, we have that $C(-x-x_j) = C(x-x_{-j})$. It follows that

$$V(-x;P\boldsymbol{v}) = \left(1/\left(\sum_{j=-M}^{M} C(-x-x_j) + C_\varepsilon\right)\right)\left(\sum_{j=-M}^{M} C(-x-x_j)v_{-j}\right) =$$

$$\left(1/\left(\sum_{j=-M}^{M} C(x-x_{-j}) + C_\varepsilon\right)\right)\left(\sum_{j=-M}^{M} C(x-x_{-j})v_{-j}\right) = V(x;\boldsymbol{v}).$$

Therefore, $\boldsymbol{U}(-x;P\boldsymbol{v}) = \frac{1}{2}\sum_{j=-M}^{M} C(-x-x_j)(v_j - V(-x;P\boldsymbol{v}))^2 = \frac{1}{2}\sum_{j=-M}^{M} C(x-x_{-j})(v_{-j} - V(-x;P\boldsymbol{v}))^2 = \frac{1}{2}\sum_{j=-M}^{M} C(x-x_j)(v_j - V(x;\boldsymbol{v}))^2$, and the proof follows by applying the chain rule on $\boldsymbol{U}(-x;P\boldsymbol{v})$. ■

Let $\boldsymbol{v} = \boldsymbol{\psi}(x)$ be the control policy for moving the chiplet in the positive direction and let x_r be a desired position. The symmetry described in the above result provides the means to generate a control pattern to move the chiplet in the negative direction, when starting from an opposite initial condition. It follows that the chiplet control policy is given by

$$\boldsymbol{v}(x) = \begin{cases} \boldsymbol{\psi}(x) & x - x_r \le 0 \\ P\boldsymbol{\psi}(-x) & x - x_r > 0, \end{cases} \tag{8}$$

where we assume that the control signal is applied at a fine enough sampling periods to allow the chiplet to get arbitrarily close to the desired position. Note that as shown in [9], there exists an upper bound on the chiplet overshoot, even in the case the sampling period is not small enough.

The capacitances and their partial derivatives are estimated by simulating a 2-dimensional electrostatic COMSOL model. In this model (Figure 2), two metal plates with dimensions given by the geometry of the chiplet and electrodes are surrounded by a dielectric with the same properties as the isopar-M solution. The quasi-static models are computed in the form of electromagnetic simulations using partial differential equations, where we use ground boundary (zero potential) as the boundary condition of the model's design. The COMSOL electrostatic model has as parameters, the

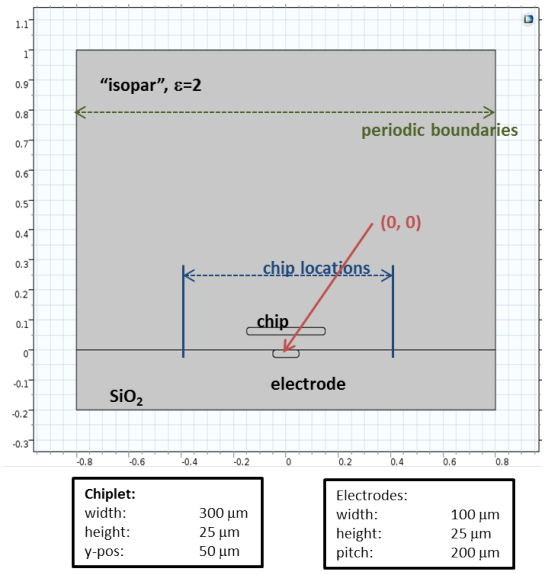

Fig. 2. Electrostatic COMSOL model of two conductors (chiplet and electrode) for capacitance computation. The electrode's position is $(0,0)$

dimensions of the chiplet and electrode, the dielectric fluid constant, and the positions of the chiplet and electrode. Note that due to the size of the chiplet versus the size of the electrodes, fringe effects (electric field distortions at the edges) are significant. The resulting capacitance function shape represented as a mixture of Gaussian functions is shown in Figure 3. As expected, the capacitance function reaches the maximum value when the chiplet is on top of the electrode and converges to zero as the chiplet moves away from the electrode. The capacitances learned via COMSOL simulations were used to learn the control patterns shown (1)-(2), which were validated through experiments. *Therefore, these functions together with model (5)-(6) represent the ground truth.*

IV. Physics (re)-learning

In this section we show how we can learn different representations for the chiplet dynamics (5)-(6), by including more and more information about the physics behind the chiplet motion. Time series of the chiplet position are considered as training data, from which velocities are approximated. These velocity estimates provide approximations of the forces acting on the chiplet. We assume zero accelerations due to the negligible chiplet mass. The time series include chiplet motion in the positive direction in the interval $[-1.8, 1.5]$ mm and 27 electrodes uniformly distributed around zero, at 0.2 mm distance from each other. For a fair comparison, the test data is generated using different initial conditions. We used Autograd [7] and Pytorch [3] (for recurrent neural network training) to learn the laws of motion for the chiplet dynamics.

Authorized licensed use limited to: Palo Alto Research Center (PARC). Downloaded on August 26,2020 at 01:39:16 UTC from IEEE Xplore. Restrictions apply.

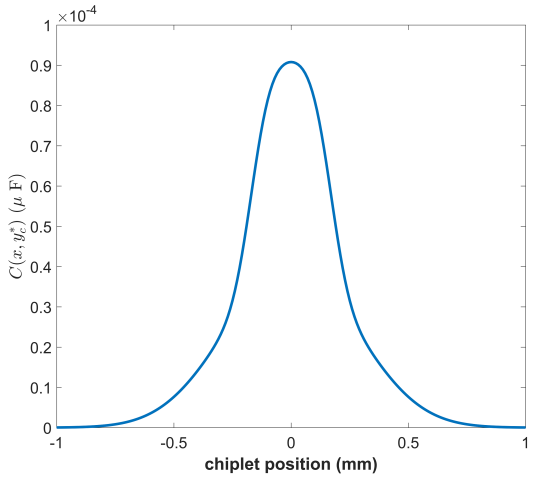

Fig. 3. The capacitance between the electrode and the chiplet as a function of the chiplet position.

Depending on the representations, we compare learned forces and potentials against the validated model, and the chiplet trajectories generated by the learned representations against the one generated by the validated model. We use as training and testing metric the relative square error (RSE), defined as $RSE(x) = \left(\sum_{i=1}^{N}(x_i - \hat{x}_i)^2\right) / \left(\sum_{i=1}^{N}(x_i - \bar{x})^2\right)$, where x_i are the target samples, $\hat{x}_i$ are the predicted values, and $\bar{x}$ is the mean of the target values. We chose this metric since the position values are measured in microns, hence even for large errors we may in fact have small numbers for the MSE metric.

In what follows we show results for a number of force and potential representations under different assumptions of what data is available/measured. Neglecting the acceleration effects, the assumed chiplet model of motion is given by

$$\mu\dot{x} = F_c(x;\beta). \tag{9}$$

The model used for learning is the discretized version of (9), namely $x(t_{k+1}) = x(t_k) + hF_c(x(t_k);\beta)$, where $h = 0.1$ msec is the sampling period and $\{t_k\}_{k\geq 0}$ are sampling instances. The learning problem solves the optimization problem

$$\min_{\beta} \sum_{k=1}^{n} |x(t_{k+1}) - x(t_k) - \frac{h}{\mu}F_c(x(t_k))|^2.$$

A. Force as a function of the chiplet position

We assume we can only track the chiplet position but not the electrodes potentials. The force model is taken as $F_c(x;\beta) = \sum_{i=1}^{N} F(x - x_i;\beta)$, representing the cumulative effect of the forces generated by the interaction with each electrode. We consider a homogeneous model for the electrode forces $F(x;\beta)$, where the changes in magnitude are given by the distance between the chiplet and the electrodes. The quantity $F(x - x_i;\beta)$ was modeled as a neural network with two hidden layers of size 500 and `tanh` as activation functions. We learn the representation for positive direction only, however the model can be used for negative direction as well. In particular, if the objective is to reach a reference point x_r we have

$$m\ddot{x} + \mu\dot{x} = \begin{cases} F_c(x;\beta) & x - x_r \leq 0, \\ -F_c(-x;\beta) & x - x_r > 0. \end{cases}$$

A graphic comparison between the learned force profile and the ground truth as a function of the chiplet position is shown in Figure 4. The training and testing results are shown in Table I.

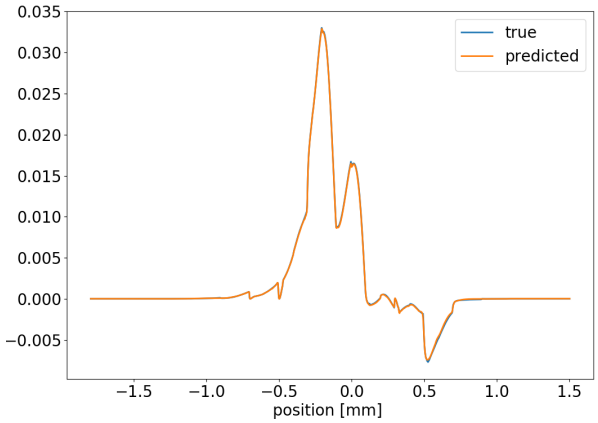

Fig. 4. The capacitance between the electrode and the chiplet as a function of the chiplet position.

B. Potential as a function of the chiplet position

Since the force is the gradient of a potential function, we can learn a representation directly for the potential function. In particular, we assume that the model of motion is $\mu\dot{x} = \frac{\partial U_c(x;\beta)}{\partial x}$, where $U_c(x;\beta) = \sum_{i=1}^{N} U(x - x_i;\beta)$, with $U(x - x_i;\beta)$ being the contribution of each electrode to the potential function. Note that when using automatic differentiation to represent the potential function gradient, the parallel processing of training data is no longer an option, hence the training process is slower. The potential function was chosen as a two layers neural network with each layer having 100 neurons and `tanh` as activation functions. The training and testing results are shown in Table I.

TABLE I
CASES A AND B TRAINING AND TESTING RESULTS

Metrics	Case A Values	Case B Values
RSE force (training)	1.46×10^{-5}	4.18×10^{-4}
RSE position (testing)	5.54×10^{-8}	5.16×10^{-6}

C. Force as a function of position and electrode potentials: recurrent neural network

We assume that we have access to electrodes potentials as well, and we model the force as a recurrent neural network (RNN) $F_c = F_c(x_{k:k-T}, v_{k:k-T};\beta)$, where $x_{k:k-T}$ and $v_{k:k-T}$ are sequences of positions and voltages of length T. In particular, we have chosen a sequence length $T = 2$ and one hidden layer of LSTM cells. The RNN was implemented and trained

Authorized licensed use limited to: Palo Alto Research Center (PARC). Downloaded on August 26,2020 at 01:39:16 UTC from IEEE Xplore. Restrictions apply.

using Pytorch. The resulting model of motion is discretized and given by: $x_{k+1} = x_k + \frac{h}{\mu} F_c(x_{k:k-T}, v_{k:k-T}; \beta)$. The training and testing results are shown in Table II.

D. Force as a function of position and electrode potentials: dense network

We have similar representations for the force model and position dynamics as in the previous case, with the difference that we now represent the force as a dense network having as input a sequence of past and present position and voltage values. The sequence length was chosen as $T = 2$, and the dense network was chosen as a two layers neural network, with hidden layers of size 20 and `tanh` as activation functions. The training and testing results are shown in Table II.

TABLE II

CASES C AND D TRAINING AND TESTING RESULTS

Metrics	Case C Values	Case D Values
RSE force (training)	1.22×10^{-2}	2.73×10^{-4}
RSE position (testing)	1.46×10^{-1}	1.43×10^{-1}

E. Force as a function of position and electrode potentials: embedded periodicity

Due to the periodic nature of the electrodes placement, the electric potential and the resulting force under the control policy are periodic as well. Hence it makes sense to include model artifacts that encourage the discovery of such property. We created a neural network model for the force that receives as input the current potential and electrode potentials that has two hidden layers of size 50 but has as activation function on the first layer a `sin` function, and a `tanh` function for the second layer. As a result, the first layer acts as a Fourier series decomposition with with unknown frequency terms, and the second layer acts a weights for the Fourier series terms that are also unknown.

F. Force as a capacitive based model

Here we model the force as an explicit representation in terms of the capacitances between the chiplet and the electrodes. In particular we have $F_c(x, v; \beta) = \frac{\partial U(x,v)}{\partial x}$, where $U(x; v) = \frac{1}{2} \sum_{j=1}^{N} C(x_j - x; \beta) \left[v_j - V(x; v)\right]^2$. The objective is to indirectly learn the capacitance model as a function of the distance between the chiplet and electrodes. The additional structure included in the force model enables us to use have simplear models that we have to learn. In particular, we use a one hidden layer of size 20 in the neural network, with `tanh` as activation functions. In addition to the force and position comparisons, we add a comparison between the predicted and learned chiplet capacitances (Figure 5).

G. Symmetry discovery

In Proposition 3.1 we showed that the chiplet dynamics is characterized by a linear discrete symmetry. We confirmed that we can indeed learn this symmetry through learning,

TABLE III

CASES E AND F TRAINING AND TESTING RESULTS

Metrics	Case E Values	Case F Values
RSE force (training)	6.65×10^{-4}	1.03×10^{-4}
RSE position (testing)	3.44×10^{-1}	4.51×10^{-7}
RSE capacitance (testing)		1.21×10^{-2}

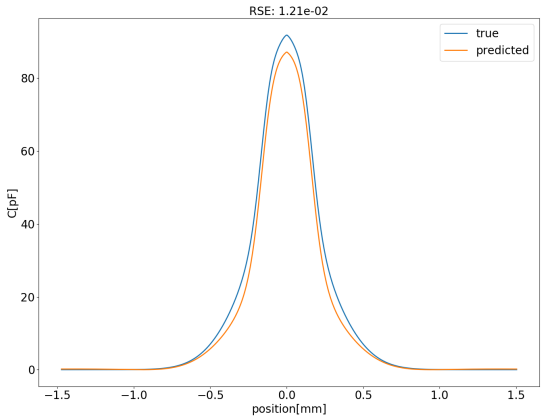

Fig. 5. True vs. learned capacitances.

directly from the data and without using the chiplet dynamics. To this end we made the assumption that the data does contain symmetrical transformations. In particular, given a data set $\mathcal{D}$ and a linear map M representing the symmetry map, $\mathcal{D}$ is invariant under the transformation M. In particular, this means that for any $z \in \mathcal{D}$, $\hat{z} = Mz \in \mathcal{D}$, as well. We recall the vector z is composed by the chiplet position, the four electrode potentials that induces the force acting on the chiplet. The symmetry learning is executed by solving the optimization problem:

$$\min_M \sum_j \min\{\|z_i - Mz_j\|^2, \forall i \neq j\} + \lambda \sum_{i,j} |m_{ij}|,$$

where $M = (m_{ij}) \in \mathbb{R}^{5\times5}$ is an unknown real matrix, and $\lambda = 10^{-5}$ is the weight for the L_1 regularization function. The test metric is the MSE between the true symmetry map and the learned one. Note that the test result may appear smaller, but the number of terms in the cost sum is much smaller as compared to the number or terms in the training cost.

TABLE IV

SYMMETRY LEARNING RESULTS

Metrics	Values
cost (training)	3.71×10^{-9}
symmetry MSE (test)	1.39×10^{-10}

H. Discussion

The learning results depend on the representation assumptions and available data. Learning the force directly

Authorized licensed use limited to: Palo Alto Research Center (PARC). Downloaded on August 26,2020 at 01:39:16 UTC from IEEE Xplore. Restrictions apply.

by ignoring the electrode potentials gave good results but cannot be generalized to other voltage patterns. Learning the potential function rather than the force is a much slower process since the loss function is in terms of the gradient of the potential function. Models with memory (e.g., recurrent neural networks) were less accurate but maintained the directional trends in the chiplet motions. The best results when considering both accuracy and generalization came from the capacitive model. This confirms our intuition that as we add more knowledge about the physical process in the representation, we end up reducing the complexity of the learning process, and the models are more generalizable. Hence. imposing the right structure into the model is key to discovering physical laws.

Extensions to multiple chiplets and 2D cases

The 1D model discussed in the previous sections can be readily extended to the 2D case. In the 2D case an array of electrodes replaces the spiral electrodes pattern. The chiplet dynamics in the 2D case is given by $m\ddot{z} = \mu\dot{z} + \nabla_z \boldsymbol{U}(z;\boldsymbol{v})$, where z is the two dimension vector of chiplet position, $\boldsymbol{U}(z;\boldsymbol{v}) = \frac{1}{2}\sum_{j=1}^{N} C(\|z_j - z\|)(v_j - V(z;\boldsymbol{v}))^2$ is the chiplet potential energy, with z_j denotes the electrodes positions. The electric potential at the chiplet has the same representation as in the 1D case. For symmetrical chiplets (e.g., spheres, cylinders), the capacitance shape can be extrapolated from the 1D case, since a cross-section looks like the capacitance in the 1D case. Figure 6 depicts an example of the capacitance between chiplets and electrodes in the 2D case. The capacitance model corresponds to cylinder shape chiplet with 300 microns diameter and 25 microns thickness. The chiplet is submerged in a dielectric fluid on top of an 50 microns pitch electrode array. For non-symmetrical chiplets,

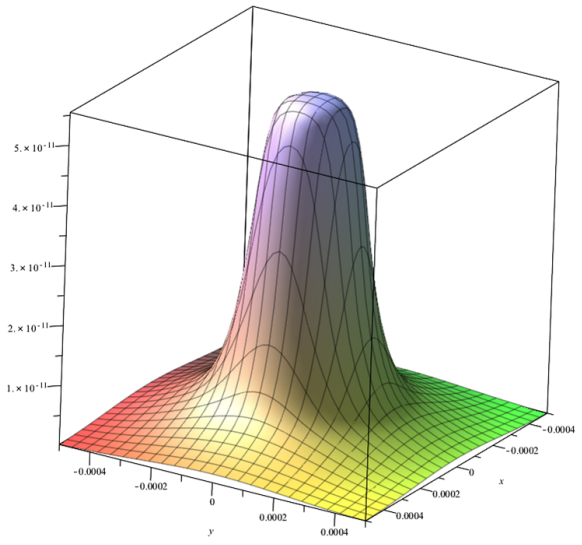

Fig. 6. Capacitance between chiplets and electrodes in the 2D case

the capacitance depends on the chiplet geometric shape and hence the chiplet orientation does matter when used in the potential energy computation. To avoid the complexity induced by the non-symmetric case, whe can approximate the chiplet shape with the closes symmetric shape, and use this capacitance model as a proxy for the real capacitance model. The inherent modeling uncertainty will be taken care through the feedback loop.

V. Conclusions

The goal of this paper was to demonstrate how ML algorithms and models can be used to discover behavioral laws of physical systems. The discovery of the physical laws governing the behavior of chiplets in dielectric fluid was used to showcase our approach. We trained a variety of ML inspired models that were circumscribed to a port-Hamiltonian representation. We sequentially imposeed additional structure in the models. The learning results confirmed our intuition that structure is key in learning generalizable and physically interpretable models. As next steps, we will extend the study to the 2D case, and more interestingly, in addition to learning chiplets to electrode interaction, we will focus on learning chiplets to chiplets interaction as well.

References

[1] J. S. Baras. Group invariance and symmetries in nonlinear control and estimation. *Nonlinear Control in the Year 2000, A. Isidori, F. Lamnabhi-Lagarrigue, W. Respondek (Edts.)*, 1:137–171, December 2000.

[2] J. Cervera, A. J. van der Schaft, and A. Baños. Interconnection of port-hamiltonian systems and composition of dirac structures. *Automatica*, 43(2):212–225, 2007.

[3] A. Paszke *et al.* Automatic differentiation in pytorch. 2017.

[4] E. M. Chow *et al.* Micro-object assembly with an optically addressed array. In *2017 19th International Conference on Solid-State Sensors, Actuators and Microsystems (TRANSDUCERS)*, pages 682–685, June 2017.

[5] J. P. Lu *et al.* Open and closed loop manipulation of charged microchiplets in an electric field. *Applied Physics Letters*, 105(5), 2014.

[6] P. E. Hydon. *Symmetry Methods for Differential Equations: A Beginner's Guide*. Cambridge Texts in Applied Mathematics. Cambridge University Press, 2000.

[7] D. Maclaurin, D. Duvenaud, and R. P. Adams. Autograd: Effortless gradients in numpy. In *ICML 2015 AutoML Workshop*, 2015.

[8] B. M. Maschke and A. J. van der Schaft. Port-controlled hamiltonian systems: Modelling origins and systemtheoretic properties. In M. Fliess, editor, *Nonlinear Control Systems Design 1992*, IFAC Symposia Series, pages 359 – 365. Pergamon, Oxford, 1993.

[9] I. Matei, S. Nelaturi, E. M. Chow, J. P. Lu, J. A. Bert, and L. S. Crawford. Micro-scale chiplets position control. *Journal of Microelectromechanical Systems*, 28(4):643–655, 2019.

[10] I. Matei, S. Nelaturi, J. P. Lu, J. A. Bert, L. S. Crawford, and E. Chow. Towards printing as an electronics manufacturing method: Micro-scale chiplet position control. In *2017 American Control Conference (ACC)*, pages 1549–1555, May 2017.

[11] A. Mouchet. Applications of Noether conservation theorem to Hamiltonian systems. *Annals of Physics*, 372, 12 2015.

[12] J. Schwichtenberg. Physics from symmetry. Springer, 2015.

[13] A. J. van der Schaft. Port-hamiltonian systems: an introductory survey. In M. Sanz-Sole, J. Soria, J.L. Varona, and J. Verdera, editors, *Proceedings of the International Congress of Mathematicians Vol. III*, number suppl 2, pages 1339–1365. European Mathematical Society Publishing House (EMS Ph), 2006.

[14] A. J. van der Schaft and D. Jeltsema. Port-hamiltonian systems theory: An introductory overview. *Foundations and Trends in Systems and Control*, 1(2-3):173–378, 2014.

[15] A. J. van der Schaft and B. M. Maschke. Port-hamiltonian systems on graphs. *SIAM Journal on Control and Optimization*, 51(2):906–937, 2013.

Authorized licensed use limited to: Palo Alto Research Center (PARC). Downloaded on August 26,2020 at 01:39:16 UTC from IEEE Xplore. Restrictions apply.